ASME Journal of Engineering for Gas Turbines and Power
Online journal at:
https://asmedigitalcollection.asme.org/gasturbinespower

Pavlos Rompokos[1]
Centre for Propulsion and Thermal Power Engineering,
Cranfield University,
College Road, Wharley End,
Bedford MK43 0AL, UK
e-mail: Pavlos.rompokos@cranfield.ac.uk

Vasileios Kyritsis
Rolls Royce plc,
P.O. Box 31, Moor Lane,
Derby DE24 8BJ, UK
e-mail: vasileios.kyritsis@rolls-royce.com

Christos Mourouzidis
Centre for Propulsion and Thermal Power Engineering,
Cranfield University,
College Rd, Wharley End,
Bedford MK43 0AL, UK

Ioannis Roumeliotis
Centre for Propulsion and Thermal Power Engineering,
Cranfield University,
College Rd, Wharley End,
Bedford MK43 0AL, UK

Assessment of a Liquid Hydrogen Conditioning System for Retrofitting on Kerosene Designed Turbofans

As energy transition to alternative fuels for civil aviation is likely to be gradual, hydrogen's first entry to service may be implemented on existing gas turbine engines. In this paper a novel liquid hydrogen conditioning system for retrofitting on kerosene designed geared turbofans is assessed in terms of performance and engine rematching. The aim of the analysis is to identify emerging requirements for the design of the fuel and thermal management system within the constraints of a certified engine design. The conditioning system proposed, an LH_2 preheater, enables the control of the gaseous hydrogen temperature at combustor entry and consists of a secondary combustor and a heat exchanger. The examined configuration considers various bleed source locations within the engine to supply the preheater system. For performing the analysis, a kerosene fueled engine has been designed and suitable integrated models capable to simulate the retrofitted hydrogen fueled engine as well as the LH_2 preheater operation have been developed. The system performance has been analyzed for the different bleed source locations identifying operating limits and performance changes. From all the examined bleed source positions, utilizing the by-pass duct minimizes the impact on component rematching and engine efficiency. Additionally, through a gas path geometry multiparametric analysis, it was found that by readjusting the capacity of the high-pressure turbine and the core nozzle area the certified limits can be met for the retrofitted engine. [DOI: 10.1115/1.4067915]

1 Introduction

Liquid hydrogen (LH_2) has long been seen as a technically feasible fuel for a decarbonized aviation future. However, its implementation poses a great challenge to both engine and airframe manufacturers as it adds complexity to aircraft and engine systems. Specifically, for the LH_2 conditioning, the industry will have to select a concept that belongs to either one of the scenarios summarized in Table 1. In particular, one criterion is whether the conditioning of the cryogenic hydrogen is happening at airframe or propulsion system level, or a combination of both. The latter scenario would impose a more integrated approach both commercially and engineering-wise between the airframe and engine manufacturers. The second criterion is whether the temperature of the conditioned gaseous hydrogen is controlled within a predefined range or varies with flight and power conditions, prior to being fed to the engine combustor.

This paper examines the scenario where the LH_2 conditioning is performed at propulsion system level aiming for controlled delivery conditions. This implementation dictates changes to the cycle and operation, due to the different combustion product properties and the increased energy requirement for LH_2 conditioning. Clean sheet engine designs may account for this from the earliest stages of development. For example, Brewer [1] suggested the pressurization of the LH_2 via a series of pumps and then its heating via several heat exchangers utilizing the heat rejection of the engine oil and environmental control system and a heat exchanger at the exhaust of the low-pressure turbine (LPT). Several subsequent LH_2 conceptual studies, such as the Cryoplane [2,3], ENABLEH2 [4], and Verstraete [5], adopted this regenerative hydrogen conditioning configuration while Abedi et al. [6] examined alternative configurations that involved compressor precooling and intercooling. As all these configurations are depended on the performance of the engine, which is driven by operational requirements, they do not offer control over the delivery conditions of the fuel.

However, an energy transition to alternative fuels for civil aviation is likely to be gradual. Operational exposure and revenue generation of H_2-powered engines will be steadily increasing, hence allowing a gradual evolution in terms of optimal integration of the LH_2 conditioning system, also accommodating in-service experience. Until then, it is likely that hydrogen's first entry to service is implemented on existing gas turbine engines via retrofitting of the fuel and thermal management systems. This is with the view of minimizing the overall exposure of a new engine to operational risks related to the integration of the new technology, but also manage the financial exposure of introducing new products [7].

The aforementioned configurations require high levels of integration with the engine and therefore are difficult to be implemented in a retrofitting scenario. Instead, this paper examines a novel LH_2 conditioning configuration, as proposed by Palmer [8],

Turbo Expo June 24–28, 2024. GT2024.
[1]Corresponding author.
Manuscript received September 23, 2024; final manuscript received February 4, 2025; published online March 18, 2025. Editor: Jerzy T. Sawicki.

Copyright © 2025 by Rolls-Royce plc; reuse license CC-BY 4.0

Table 1 Potential solutions for LH_2 conditioning

Criterion	Scenarios		
Conditioning unit	Propulsion system	Airframe	Combined airframe—engine
Delivery conditions	Controlled within range	Fluctuating upon operating condition	Combined

Tacconi and Grech [9], capable of providing adequate control over the hydrogen delivery conditions regardless the operating setting of the engine. Specifically, the system consists of a parallel hydrogen combustion (PHC) system to the main combustion chamber of the engine fed by engine bleed flow. The paper addresses the feasibility of this concept in a retrofitting scenario that has not been considered before with the view of identifying emerging requirements and discussing performance and operational aspects.

Firstly, good practices for H_2-fueled gas turbine modeling are presented. Then the baseline Jet A-1 fueled cycle design is introduced and the performance of the cycle for hydrogen without any fuel conditioning is analyzed, highlighting the fuel and components rematching effects. Then the PHC model is coupled with the baseline engine model. A multitude of air-source locations are considered in the core and the bypass streams and the H_2-fueled engine attributes are assessed for the same thrust duty and compared against the kerosene-defined mechanical speed and temperature limits. The performance and operation of the integrated fuel and engine system are calculated, and penalties are quantified. Finally, the least penalizing from a thermodynamic cycle viewpoint PHC air-source is down-selected and hot section capacity changes are explored for ensuring operation within the mechanical speed and temperature limits of the baseline engine.

2 Assumptions

The paper carries out a preliminary exploration of the operational envelope of the engine and the PHC considering a multitude of PHC air-source locations. The objective is to identify emerging requirements and/or system restrictions for the PHC, with a view to assessing the viability of the proposed solution. In doing so, simplifications have been considered, which are listed hereafter:

1. A one-dimensional performance solver is used, i.e., PROOSIS. As such two and three-dimensional flow effects, e.g., due to the extraction of bleed and/or changes in combustor exit traverse, have not been considered on turbomachinery performance and air-system source static pressures.
2. The HP compressor characteristic is assumed not to change with interstage bleed. The assumption, while not technically true, enables the investigation of the thermodynamic cycle response, without investigating the effects of interstage bleed on HPC efficiency, capacity and surge margin.
3. Air-system flow consumption is assumed a fixed fraction of core flow. The assumption grants realistic results as long as secondary air-system driving pressure ratios vary within the range of a power curve.
4. Turbine cooling flow rates are also assumed a fixed fraction of core flow, despite potential changes in temperature deltas between the gas path and the cooling flows, potential changes in heat transfer characteristics and vane-coating materials to address the increased water vapor threat.
5. No change in HPT effective capacity is considered, because of a potential change in the combustor exit traverse. Such a profile change is possible due to combustor modifications to facilitate optimal GH_2 combustion with a view to efficiency and emissions.
6. Ideal behavior of the liquid hydrogen pump is assumed, i.e. lack of thermo-mechanical or hydraulic side-effects, such as cavitation of saturated liquid hydrogen at pump entry.
7. The heat-load requirement for the gasification of liquid hydrogen is fully attributed to the pre-heater. In practice, the fuel line may lend itself to a more conventional use as a heat sink for other thermo-fluid systems in the engine, such as cooling of oil, cooling of hydraulic fluids used for actuation, e.g., the VIGV/VSV mechanisms, and cooling of Variable Frequency Generators. Such an approach has the potential to slightly reduce the heat-dissipation requirement of the LH_2 conditioning system [1], at the expense of extra complexity and failure modes to be considered. The assumption of conditioning the fuel solely via the preheater is a simplification to aid modeling. The assumption is validated acknowledging that the heat dissipation requirement for the gasification of liquid hydrogen at the required fuel flowrates is of the order of 1-2 MW, while the thermofluid-system sinks would serve heat dissipation of the order of a few hundreds of kW.

The assumptions covering the aerothermal engine behavior shall be cross-examined against the recommended preheater bleed source, assessing whether such an installation would severely invalidate them.

3 Hydrogen Fueled Gas Turbine Modelling

For modeling a hydrogen fueled engine cycle the following aspects should be considered: the lower heating value (LHV), which affects the combustion chamber equilibrium, the combustion product properties, which affect the gas path performance and may affect turbine map characteristics, depending on how they were generated, and the pure hydrogen properties, which affect the performance of the fuel conditioning system.

Hydrogen upon combustion releases 120 MJ for every kg burnt, whereas for the same quantity, conventional Jet A-1 releases 43.2 MJ [10]. For a jet engine, and considering the same compressor power requirement, the combustion equilibrium would suggest a reduction in fuel consumption between H_2 and Jet A-1 similar to the ratio of their lower heating values (LHV), i.e., approximately 64%. Apart from the LHV of the fuels, the combustion product properties of H_2 also differ from that of Jet A-1. The ones that affect the performance of the engine are the specific heat capacities (Cp), the heat capacity ratios (γ), specific enthalpies, specific entropies, and the gas constant (R). Herein these properties were produced using NASA's CEA software [11] and were tabulated according to the temperature of the flow and burnt fuel-to-air ratio (FAR).

Considering the Cp, for example, for gasses with combustion products of Jet A-1 and H_2, the Cp for a FAR of 2% at a temperature of 1500 K is 1257 J/kg K and 1470 J/kg K, respectively. Although the difference between the two gas properties is significant ($\sim$16% increase for H_2), the properties of the two flows can be better characterized with equivalent FAR due to the reduction in fuel burn in the combustion chamber. Hence, in Fig. 1, the Cp against temperature for dry air, Jet A-1 at 2% FAR and H_2 at 0.75% FAR are presented. In this scenario, gasses with H_2 combustion products, on average, have a 3.9% higher Cp than conventional kerosene. This potentially increases the efficiency of the engine as it reduces the temperature drop in the turbines for the same enthalpy increase requirement in the compressors. R shows a similar to the Cp increase due to the higher water vapor content in the gasses; 300.2 J/kg K for 0.75% FAR of H_2 while 287 J/kg K for Jet A-1.

γ against temperature and FAR for H_2 and Jet A-1 gas mixtures is presented in Fig. 2. Contrary to Cp and R, γ properties between the two cases do not show significant change and therefore differences in the flow expansion at the turbines would have a minor effect on the engine performance.

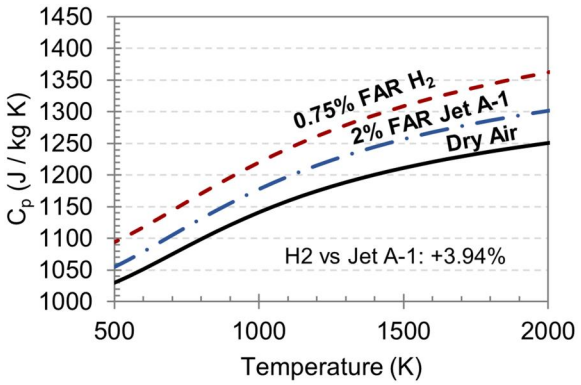

Fig. 1 Cp over temperature for dry air, Jet A-1 and H_2

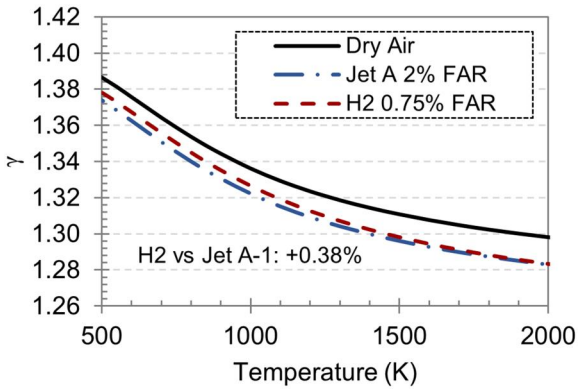

Fig. 2 γ over operating temperature for dry air, Jet A-1 and H_2

Change in the flue gas properties affects the expansion as well if the turbine geometry is unchanged. In order to consider this phenomenon in the context of 0_D performance models suitable turbine map corrections should be applied. Such correction factors were proposed by the Advisory Group for Aerospace Research and Development [12] and were intended to account for the effect of water injection on the performance of the turbomachinery components. These, however, are also relevant in the case of modeling with different fuels. They involve corrections for the corrected rotational speed (Nc), corrected mass flow (Wc) and enthalpy change to inlet temperature ratio, as shown in Eqs. (1)–(3), respectively (where i and map are the actual and reference map gas path properties, respectively). These have been derived by considering similarity in the velocity triangles and that the turbines operate at chocked conditions. For reference the Nc and Wc are determined as discussed by Volponi [13] as shown in Eq. (4)

$$\frac{\mathrm{Nc}_i}{\mathrm{Nc}_{\mathrm{map}}} = \sqrt{\frac{R_i\gamma_i(1+\gamma_{\mathrm{map}})}{R_{\mathrm{map}}\gamma_{\mathrm{map}}(1+\gamma_i)}} \tag{1}$$

$$\frac{\mathrm{Wc}_i}{\mathrm{Wc}_{\mathrm{map}}} = \sqrt{\frac{\gamma_i R_{\mathrm{map}}}{\gamma_{\mathrm{map}} R_i}}\left(\frac{\gamma_{\mathrm{map}}+1}{2}\right)^{\frac{\gamma_{\mathrm{map}}+1}{2(\gamma_{\mathrm{map}}-1)}}\left(\frac{2}{\gamma_i+1}\right)^{\frac{\gamma_i+1}{2(\gamma_i-1)}} \tag{2}$$

$$\frac{(\Delta h/T)_i}{(\Delta h/T)_{\mathrm{map}}} = \frac{R_i\gamma_i(1+\gamma_{\mathrm{map}})}{R_{\mathrm{map}}\gamma_{\mathrm{map}}(1+\gamma_i)} \tag{3}$$

$$\theta = \frac{T}{T_{\mathrm{ref}}},\ \delta = \frac{P}{P_{\mathrm{ref}}},\ Wc = W\frac{\sqrt{\theta}}{\delta},\ Nc = \frac{N}{\sqrt{\theta}} \tag{4}$$

4 Hydrogen Fueled Gas Turbine Modelling

For the performance simulations of the baseline model and its variations, the Propulsion Object Oriented Simulation Software (PROOSIS) was used. This is a simulation platform capable of multidisciplinary system modeling and in particular gas turbine systems and is being widely used across academia and industry [14–18].

Table 2 Thrust requirements across design operating points

Operating point	MCR (DP)	ToC	EoR	SLS idle
FN (kN)	20.1	24.3	94.7	14.4
Mn	0.78	0.78	0.25	0
Altitude (kft)	35	35	0	0
dT_{ISA} (K)	0	+10	+15	0

The test case that is selected is targeting the short-to-medium range applications similar to the Airbus A320 or Boeing 737 family of aircraft with an entry into service 2030. The thrust requirements for such an application are adopted by another conceptual study as discussed by Alexiou et al. [19]. The engine configuration is a geared turbofan with a fixed by-pass (BP) nozzle area. It features a high-pressure spool that connects the high-pressure turbine (HPT) to the high-pressure compressor (HPC) and a low-pressure spool that connects the low-pressure turbine (LPT) to the low-pressure compressor (LPC) and in turn drives a planetary gearbox that powers the fan. The engine thrust ratings for four representative points are presented in Table 2 [19]. The engine cycle is designed according to the requirements of the three key operating conditions, midcruise (MCR), top of climb (ToC), and end of runway (EoR), following a multipoint cycle design approach. The sea level static (SLS) idle setting, although is not included in the design process, it will be considered subsequently for the performance assessment of the LH_2 conditioning system.

For the multipoint cycle design, MCR is set as the design point (DP) where turbomachinery maps and nozzle areas are scaled and then ToC and EoR are simulated at off-design (OD). The approach followed targets to maximize both the turbine entry temperature (TET) and overall pressure ratio (OPR) by matching a set of maximum temperature targets across any of the three operating conditions. On a geared turbofan for SMR applications, maximum allowable temperature limits are met during EoR conditions, where both TET and the compressor exit temperature T3 reach their peak values. In addition, the fan diameter is estimated at ToC as it operates at its maximum flow capacity.

At the DP calculation, the turbomachinery component efficiencies and fan pressure ratio (FPR) are set as direct inputs from Ref. [19]. In addition, initial guesses of TET and OPR are assumed while the ratio between the LPC to HPC pressure ratio is fixed. The by-pass ratio (BPR) is then optimized based on minimum specific fuel consumption (SFC) at DP. Then the EoR performance is simulated and the whole process is iterated by correcting the combination of DP TET and OPR so that they satisfy the temperature limits set. Finally, the ToC performance is estimated, and the engine fan diameter is sized based on representative inlet Mach number and hub-to-tip ratio (HTR). The DP input efficiencies as well as cycle temperature limits are presented in Table 3. In addition, as a first order approximation for all three operating points, constant power off-take is assumed to account for the auxiliary system power requirements [19] as well as interstage HPC bleed for the environmental control system (ECS) feed as discussed in Ref. [20]. The cooling flow fractions for the turbines also set representative values to ensure that the turbine blade metal temperature limits are not exceeded [21].

Based on the discussed process, every FPR results in a different design and the final selection was based on optimum MCR SFC. The performance of the selected model for the three operating conditions is summarized in Table 4. The selected model has an MCR FPR of 1.33, which corresponds to the maximum allowed fan diameter. The optimum BPR is 15.9 while the FAR at the combustor exit is 2.2%. The energy specific fuel consumption (ESFC) is 608 W/N at Cruise, which is calculated as the ratio between the thermal energy of the fuel that is released upon combustion to the net thrust of the engine.

Table 3 Multipoint-design input parameters and constraints

MCR inputs					
$\eta_{polytropic}$			$\eta_{isentropic}$		PR_{LPC} / PR_{HPC}
FAN	LPC	HPC	HPT	LPT	
0.957	0.906	0.903	0.917	0.933	0.3

Constraints				
EoR		ToC		
TET_{max} (K)	$T3_{max}$ (K)	$D_{Fan,max}$ (m)	$Mn_{Fan,in}$	HTR_{Fan}
1850	950	2.0	0.65	0.3

Constant parameters			
$PW_{off\text{-}take}$ (kW)	W_{ECS} (kg/s)	$W_{HPT,cooling}/W_{HPC,in}$	$W_{LPT,cooling}/W_{HPC,in}$
100	1	12.5%	2.5%

This will be relevant for the later part of the paper where the engine performance using hydrogen will be compared against this baseline Jet A-1 model.

Following the definition of the baseline model, the next step is to analyze its performance for gaseous hydrogen (GH_2) without fuel conditioning to identify the effect of fuel properties and map change on the cycle rematching and performance. In this case, the GH_2 is considered to be provided readily conditioned at the combustor component to a temperature of 250 K. The engine model is configured to run at off-design for the same thrust requirements summarized in Table 2. In this way, the engine hardware, as defined by the sized turbomachinery maps and nozzle areas for Jet A-1, are maintained the same.

Figure 3(*a*) presents the engine rematching in terms of PR, Wc and Nc for all the turbomachinery components without accounting for the gas properties corrections discussed in Sec. 3. Figure 3(*b*) shows the engine rematching with these corrections and it can be concluded that the changes in turbomachinery performance parameters are different by more than a fraction of a percent. This observation is making the proper implementation of gas property corrections on turbomachinery characteristics mandatory in the analysis presented hereafter.

The difference in performance between H_2 and Jet A-1 of the engine for the three operating conditions is presented in Table 5. Most notably the fuel flow WF reduces by 64% which approximately matches the LHV ratio between the two fuels; an equivalent reduction in FAR is also observed, as at MCR at the combustor exit, it is 0.8%. However, a further heat input reduction is observed when looking at ESFC for the reasons explained below.

The change to H_2 fuel results in increased water content in the combustion gas. The latter translates to a reduction of the molecular weight of the combustion gas and an increase in its gas constant and

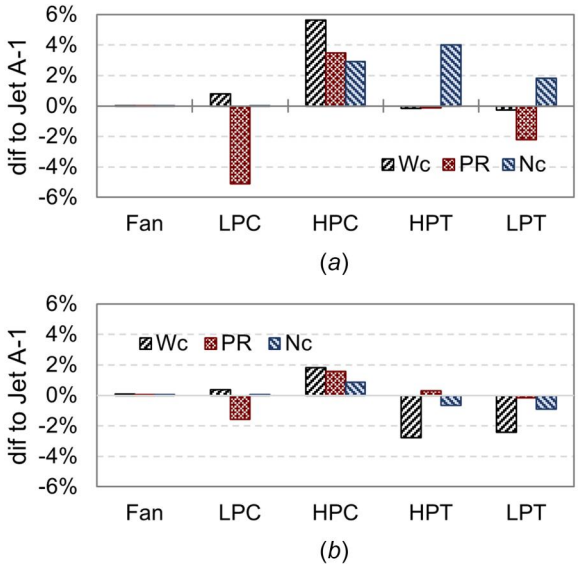

Fig. 3 End of runway turbomachinery component performance comparison between H_2 and Jet A-1 without (*a*) and with (*b*) gas properties map corrections

specific heat capacity. Physically interpreting the rise in specific heat capacity, the combustion gas can provide the same amount of power during an adiabatic expansion with a smaller temperature drop. This cascades into increased temperatures at the exit of the HP turbine, i.e., the entry of the LP turbine, and hence increased LP turbine power output for the same expansion ratio. The increased power output is further exacerbated by the increased heat capacity; both entry temperature and heat capacity being shown in Eq. (7). This is derived by considering that the generated turbine power is described by Eq. (5) and the definition of Cp in Eq. (6)

$$\mathrm{PW} = \eta_T W C_p T_{in}\left(1 - \frac{1}{ER^{\frac{\gamma-1}{\gamma}}}\right) \tag{5}$$

$$C_p = \frac{\gamma}{\gamma - 1}R \tag{6}$$

$$\mathrm{PW} = \eta_T \underbrace{\left(\frac{W\sqrt{T}}{\mathrm{PA}}\right)\sqrt{\frac{R}{\gamma}}}_{\substack{\text{Turbine}\\ \text{Capacity}}} \cdot \underbrace{\frac{\gamma\sqrt{\gamma R}}{\gamma - 1}}_{\substack{\text{Gas}\\ \text{Properties}}} \cdot \underbrace{A}_{\substack{\text{Turbine}\\ \text{Area}}} \cdot \underbrace{P\sqrt{T}}_{\substack{\text{TurbineEntry}\\ \text{Conditions}}} \cdot \underbrace{\left(1 - \frac{1}{\mathrm{ER}^{\frac{\gamma-1}{\gamma}}}\right)}_{\substack{\text{Turbine}\\ \text{Expansion}}} \tag{7}$$

Table 4 Jet A-1 baseline model results

Parameter operating point	Units	MCR	ToC	EoR
OPR		41.18	45.60	40.10
FPR		1.33	1.38	1.31
TET	K	1547	1732	1850
T3	K	786	861	950
W1	kg/s	269	272	633
WF	kg/s	0.284	0.349	0.929
V_{Core}/V_{BP}		1.13	1.28	1.21
SFC	g/(kN·s)	14.11	14.49	9.81
ESFC	W/N	608	625	423

Table 5 Relative differences between LH_2 w/o fuel conditioning and Jet A-1 baseline performance comparison

Operating point	MCR	ToC	EoR
OPR	0.1%	0.0%	−0.1%
FPR	0.1%	0.1%	0.0%
TET	−2.5%	−2.7%	−3.4%
T3	0.2%	0.5%	0.0%
W1	0.1%	0.1%	0.1%
WF	−64.7%	−64.7%	−64.9%
V_{Core}/V_{BP}	−0.3%	−0.3%	−0.4%
SFC	−64.7%	−64.7%	−64.9%
ESFC	−1.7%	−1.8%	−2.3%

In order to maintain approximately the same power requirement to the fan at a fixed thrust, the entry temperature to the LPT has to be reduced and that is accommodated by a throttle back of the fuel flow and the combustor exit temperature. The justification is summarized as 3.4% drop in TET at EoR which is approximately equivalent to 65 K.

The reduction in core-exhaust gas-temperature also affects the hot-to-cold jet velocity ratio, which is now reduced below its optimal value. That contribution of cycle inefficiency at engine level is reflected as a drop in propulsive efficiency and is accommodated by the increased overall engine mass-flow at 0.1% practically across all flight conditions examined.

A better insight into the overall engine performance with GH_2 can be obtained by examining the individual turbomachinery component performance in the core. Looking at the expansion ratio of the HP and LP rubines this not much affected, due to their operation largely between fixed capacities and the small change in γ as depicted in Fig. 2. However, the increased Cp of the exhaust gas is causing a shift in the HP compressor working line, which is translated to a shift in Wc, Nc and PR all being around or above 1%, as per Fig. 3(*b*). Given that the IP compressor is coupled to LP shaft, its mechanical speed is almost unaffected at a 0.1% increase. That results in a drop of the PR_{LPC}, as the corrected mass-flow at its exit is increased. With a change in the compression split, the PR_{LPC} drop is counterbalancing the PRHPC increase, and the overall compression PR remains practically unaffected. From these results it is apparent that switching from kerosene to hydrogen results to component rematching that may affect operation (e.g., increase of shafts speeds for EoR). At the same time a performance benefit is predicted, which is expected to be negated when LH_2 conditioning is considered. The LH_2 conditioning system considered herein is described in Sec. 5.

5 LH_2 Conditioning With Parallel Hydrogen Combustion

The primary functionality of the PHC module is the conditioning of the cryogenic H_2 stored in the LH_2 tank to adequate pressure and temperature levels. The PHC module consists of a gas line and a H_2 line. The gas line is fed with air sourced from the engine compression system via a manifold, which is further modulated via a downstream pressure-regulating valve at off-design conditions. The regulated air is then com busted in the SC prior to entering the air-H_2 Heat Exchanger and being exhausted via a nozzle. The H_2-line is supplied with LH_2 from the cryogenic H_2 tanks. The LH_2 is pumped at adequate pressure for later use in the engine fuel system, hence reaching supercritical state. The pumped H_2 is then heated via the air-H_2 heat exchanger to target temperature levels. The conditioned fuel flow then splits into two parts, one that goes to the primary combustor (PC) of the engine and another that is directed to the SC.

Figure 4 provides a diagrammatic depiction of the PHC module as developed in PROOSIS. To model the fuel system performance and its impact on the engine cycle, relevant components were developed to expand the capabilities of PROOSIS. These were a fuel-to-air heat exchanger, a fuel pump and the gas property module; relevant details are provided in the sections hereafter.

5.1 Parallel Hydrogen Combustion System Modelling. For the fuel side, pure LH_2 properties such as specific enthalpy, specific entropy, and Cp, were generated from Ref. [22] and tabulated against temperature and pressure of the flow. The data cover a wide range of operating conditions from cryogenic liquid/gaseous to supercritical phases, 1–400 bar and 20–800 K, and are more densely populated toward the saturation conditions to capture the complex topology of the phase transition region.

The objective of the pump component is to increase the pressure of the hydrogen extracted in liquid phase from the cryogenic tank. The mechanical power consumed as part of the process is accounted as mechanical off-take from the HP shaft. The pump delivery pressure is defined as twice the pressure at of the core flow at the inlet of the PC as a first approximation, as a means of accommodating for losses in the fuel system and ensuring adequate pressure ratio at fuel ejector. As such, H_2 ends up in supercritical state at the exit of the pump for all operating points considered in this study. Given user-defined pump transfer and isentropic efficiencies, fuel enthalpy rise and mechanical power requirement are then calculated. In PROOSIS the pump component is equipped with a fuel port and a mechanical port to connect with other fuel system and power transfer components, respectively. For the purposes of this study, the pump is assumed to receive liquid hydrogen at saturated conditions of 21 K and 1.5 bar from the cryogenic LH_2 tank and the isentropic and transfer efficiencies have been set to 0.5 and 0.9, respectively.

The heat exchanger transfers heat from the gas line to the supercritical H_2 flow. This is modeled in a manner agnostic to the geometry, to capture the top-level performance. More precisely, it accounts for the heat balance between the two flows, presented in Eq. (8), according to the cold and hot side mass flowrate (W_{cold}, W_{hot}), the temperature drop of the two sides ($T_{hot,in} - T_{hot,out}$, $T_{cold,in} - T_{cold,out}$) and the mean specific heat capacities (Cp cold, Cp hot) between the inlet and the outlet of the two streams. In addition, it also accounts for the heat exchanger effectiveness (ε_{HX}), shown in Eq. (9). In the calculations that take place during each iteration, gas and H_2 inlet and outlet properties are inputs to the PHC-module, as well as the heat exchanger effectiveness (ε_{HX}), which is assumed constant as a first-order approximation. As such, Eqs. (8)–(10) form a system of four equations with four unknown quantities, in particular the heat flux, the cold and hot mass-flow rates and C_{min}. In PROOSIS the Heat Exchanger component shares the flow properties via a flow port and a fuel port that are compatible with the connected components. For the purposes of this study the heat exchanger effectiveness (ε_{HX}) has been assumed at 0.25.

$$W_{hot}Cp_{hot}(T_{hot,in} - T_{hot,out}) = W_{cold}Cp_{cold}(T_{cold,out} - T_{cold,in}) = q_{HX} \tag{8}$$

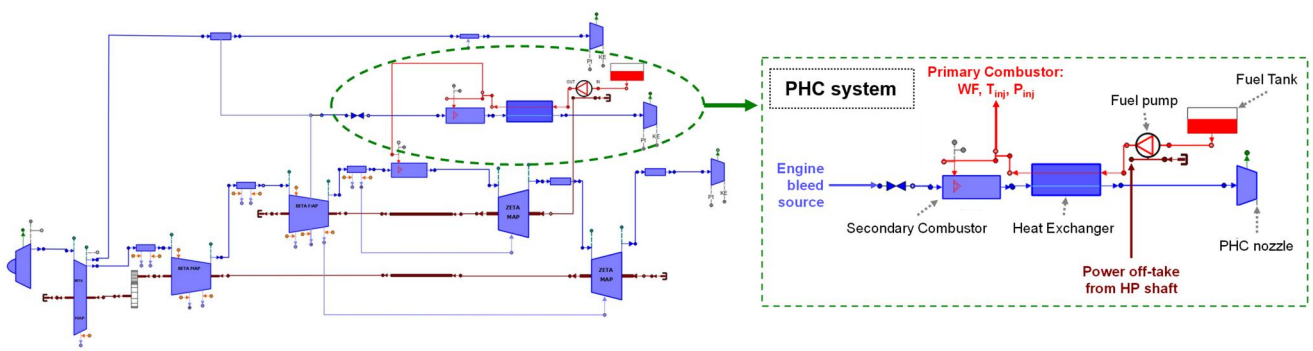

Fig. 4 Parallel hydrogen combustion integration with the engine model in PROOSIS

$$\varepsilon_{HX} = \frac{q_{\mathrm{HX}}}{C_{\min}(T_{\mathrm{hot,in}} - T_{\mathrm{cold,in}})} \tag{9}$$

$$C_{\min} = \min(Cp_{\mathrm{cold}} W_{\mathrm{cold}}, Cp_{\mathrm{hot}} W_{\mathrm{hot}}) \tag{10}$$

5.2 Sizing and Control Logic of the Parallel Hydrogen Combustion-Module Off-Design. The PHC module aims to deliver H_2 at the exit of the Heat Exchanger at a set temperature, regardless of the operating conditions of the engine. In controlling the fuel-flow temperature, the secondary combustor (SC) is also designed to operate at a fixed outlet temperature. To achieve that, two other parameters are modulated, the gas-line airflow-rate and the fuel flowrate into the SC. The gas-line airflow rate is physically modulated by actuation of the air-valve upstream of the SC and downstream of the bleed manifold; the air-valve schedule will be discussed in Sec. 5.3. For the calculations discussed hereafter, the fuel H_2 temperature at Heat Exchanger exit is assumed at 250 K, while the Secondary Combustor Outlet Temperature is set at 1000 K; that is with a view to the material limitations of a pressure vessel without elaborate cooling technology.

To simulate the integrated performance of the PHC with the engine, two types of calculations are considered, the design point and the off-design. During the former the nozzle exit area of the PHC is sized while the pressure valve component is fully open (i.e., not imposing pressure losses). At off-design, the nozzle area calculated at Design Point is used, while the pressure air-valve has a variable position for mass flow regulation. In all cases, the performance of the integrated model is calculated according to the ambient conditions and thrust requirements of Table 2 as well as the PHC control temperatures discussed above. It is also noted that the residual thrust from the PHC nozzle is not accounted for in the overall thrust requirement.

5.3 Integrated Engine—Parallel Hydrogen Combustion Integrated Performance Analysis. In this section, the performance of the integrated propulsion system (engine and LH_2 conditioning system) for different air sources for the PHC is presented and compared against the baseline Jet A-1 cycle for the four key operating points presented in Table 2.

End of runway is the condition where the highest engine fuel flow is met; hence, the condition with the highest amount of heat required to condition the cryogenic LH_2. This makes EoR the sizing operating condition for the PHC. The following analysis presents the sizing cases for various bleed locations, which are examined parametrically. Such bleed locations are the bypass duct, the inlet or exit of the HP compressor or any interstage location of the HP compressor.

In Fig. 5, the total H_2 requirement (WF_{tot}) and the PC (WF_{PC}) are presented against the various bleed source positions. The WF_{PC} increases with increasing bleed air-pressure, as more power is required to compress the additional air that is not used for thrust generation. At the same time, the fuel flow of the secondary combustor (WF_{SC}) reduces since the air is introduced at higher temperatures. Overall, the combined effect increases the WF_{tot} for the same thrust requirement when bleeding from the later stages of the HPC.

The heat exchanger operates at almost constant temperature differences between the two sides. The cold side ΔT_{cold} is 215 K since the pump delivery conditions are similar for all cases and the delivery temperature at the combustors is controlled at 250 K. At the hot side, the inlet temperature is also controlled at 1000 K and since the ε_{HX} is constant for all the cases the ΔT_{hot} is approximately 241 K. Therefore, any increase in the WF_{tot} requires an increase in PHC mass flow requirement. This is observed in Fig. 6, where the lowest W_{PHC} is required when air is sourced from the bypass duct. In the same figure, the inlet diameter of the secondary combustor (D_{SC}) is also presented. This was calculated based on the inlet flow conditions assuming entry Mach number of 0.07. The diameter of the SC varies inversely to the pressure of the airflow combusted, hence posing an increasing challenge of physical integration at reducing air-source pressures.

The nozzle pressure ratio of the PHC (NPR_{PHC}) is shown in Fig. 7. Expectedly, when air is extracted from the higher HPC stages, it has a high potential energy and since it is not expanded in the turbines, maintains that energy at the exit. If we considered an ideal expansion in the PHC nozzle, the gross thrust generated from the exit flow would contribute up to 3.6% of the net thrust. It is acknowledged that this is a theoretical calculation and does not reflect a practical scenario, given mechanical and noise constraints of the ventilation nozzle, via which such a flow would be exhausted from.

The power requirement of the fuel pump depends on the absolute LH_2 flowrate and the pressure rise required; the latter varies proportionally to the engine OPR which sets the combustor pressure levels. As shown in Fig. 7, when extracting air from the core, the required pump power increases when extracting air from later HPC stages, as the increase in H_2 fuel flow fully compensates for the reducing combustor pressure at a thrust. Extracting air from the BP duct results in a relatively increased power requirement, when compared to sourcing air from HPC, mainly due to the higher OPR dictated by the engine rematching (approximately 40 for the BP bleed and 38.5 for the HPC bleed sources). Considering the overall HPC power requirement, the pump power accounts for approximately 0.5% of the HP shaft power, which is equivalent to the auxiliary power extraction considered for other systems. Consequently, should the pump be connected to the auxiliary gearbox of the engine, this would require a redesign to account for the additional load requirement.

To obtain a better perspective of the PHC mass-flow consumption, the mass-flow ratio of the PHC to the HPC inlet is shown in Fig. 8, across all operating points. At EoR this is the highest accounting for up to 10% of the HPC inlet mass flow, and hence setting it as the PHC sizing point. The airflow consumption reduces at ToC, MCR, and SLS idle, however, it remains a considerable amount of bled air. Bleeding air from the BP requires an equivalent amount of W_{PHC}, but comes with the advantage of leaving the core

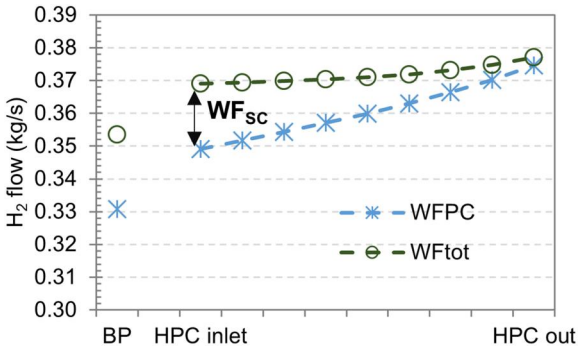

Fig. 5 Primary combustor and total H_2 flow over bleed source position at EoR

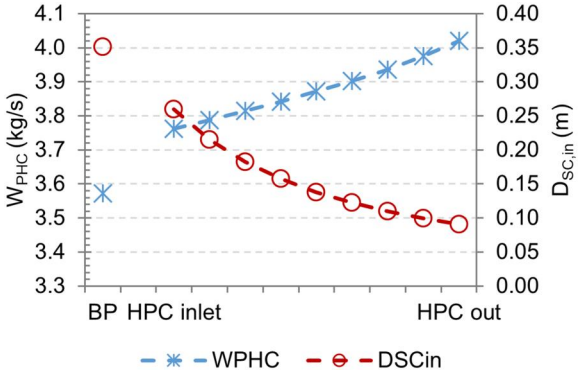

Fig. 6 Parallel hydrogen combustion inlet mass flow and diameter over bleed source position at EoR

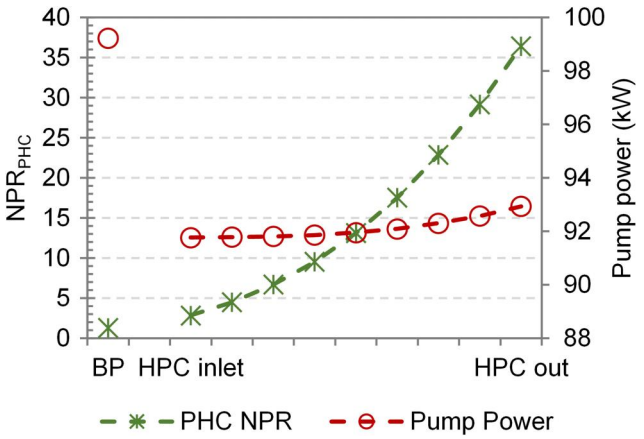

Fig. 7 Parallel hydrogen combustion nozzle pressure ratio and fuel pump power requirement over bleed source position at EoR

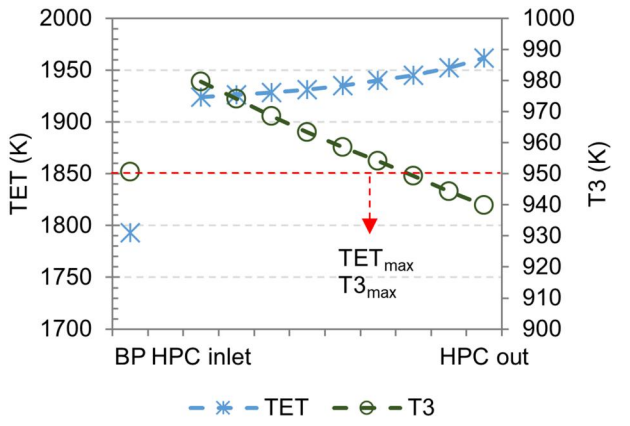

Fig. 9 Turbine entry temperature and T3 for the integrated PHC engine cycle at EoR

engine unaffected. This is considering the impact on the rematching of the LPC and HPC work split in case of core bleed, and also the rematching of the HPC front and rear stages in case of HPC interstage bleed. In extension, this has a considerable effect on the TET, as shown in Fig. 9, as sourcing air for the PHC from core leads to a significant increase in TET, exceeding as such the limits set for the baseline Jet A-1 cycle. Sourcing air from the BP avoids this and allows for 50 K margin.

The breakdown of the efficiencies of the different PHC cycles can be summarized by the respective propulsive and thermal efficiencies as well as the ESFC at MCR as shown in Figs. 10 and 11. The propulsive efficiency shows a small change across the various bleed sources since the assessment is at fixed thrust and engine diameter. The descending trend toward the last HPC stages is due to the increase in V_{core} to V_{BP} ratio away from its ideal value; it is associated with the increasing temperature and velocity at the hot nozzle. The ESFC is then mainly influenced by the thermal efficiency which follows WF_{tot} variation.

Apart from the W_{PHC}, the PHC delivery pressure is also an important factor for the scheduling of the fuel conditioning module. In Fig. 12, the pressure losses imposed by the flow control valve for all the operating points are presented, where 0% corresponds to the valve being fully open and +100% fully closed. At EoR the pressure losses are set to 0 to size the nozzle area, and at any other condition the air-valve position is varied. At ToC, when air from the early stages of the HPC is used for the PHC, the valve is almost fully open, and the maximum flow capacity is delivered to the fuel conditioning module. At SLS idle, bleeds from the HPC can adequately supply the PHC with pressurized air, however, the BP supply pressure is lower than what the PHC requires, hence the negative value. For this case, the PHC needs to be supplied from another source, hence setting a system restriction and an emerging requirement for system design.

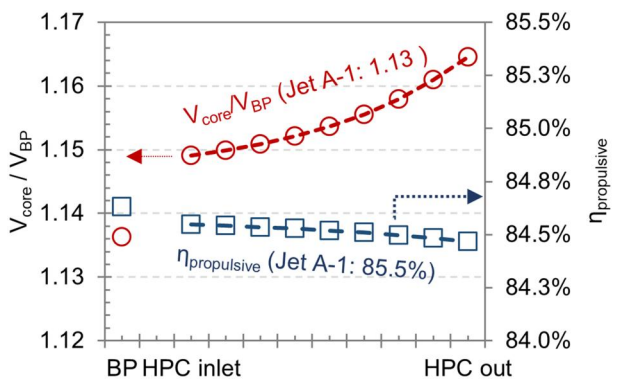

Fig. 10 Jet velocity ratio and propulsive efficiency for the PHC engine cycles at MCR

Finally, the rotational speed difference to the baseline of both shafts for the BP, HPC inlet and outlet source positions are presented in in Table 6. All solutions exceed the baseline values, however the minimum impact is achieved when air from the BP is sourced.

From the examined configurations, sourcing air for the PHC from the BP duct appears as the best thermodynamic and aerodynamic solution since it achieves the lowest ESFC and does not exceed TET limits. However, it comes with physical integration difficulties and operational challenges at low power-settings at SLS. In addition, the shaft speeds are certified limits ensuring the mechanical integrity of the turbomachinery components and the containment capability of their casings. Section 6 aims to address this issue for the BP source solution by considering changes in the capacity of the HPT and the core nozzle.

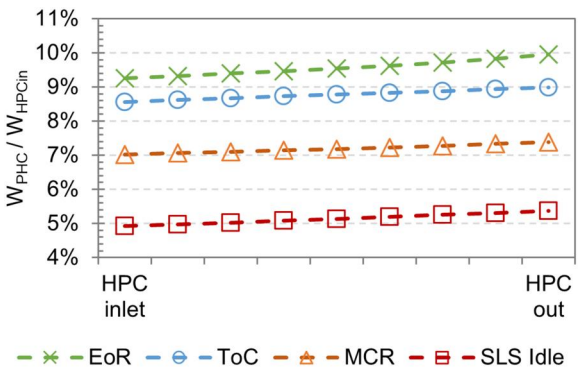

Fig. 8 Parallel hydrogen combustion to HPC inlet ratio of mass flows for various operating conditions over bleed source position

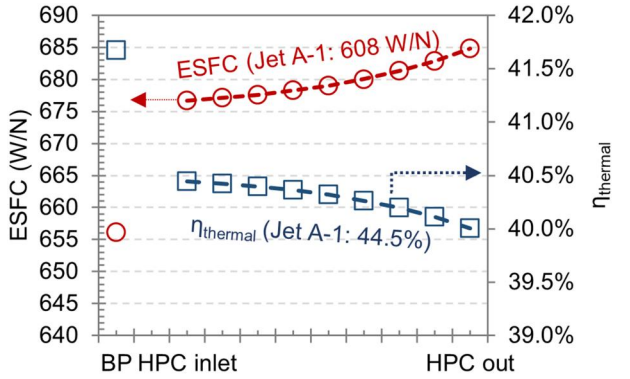

Fig. 11 Thermal efficiency and ESFC for the PHC engine cycles at MCR

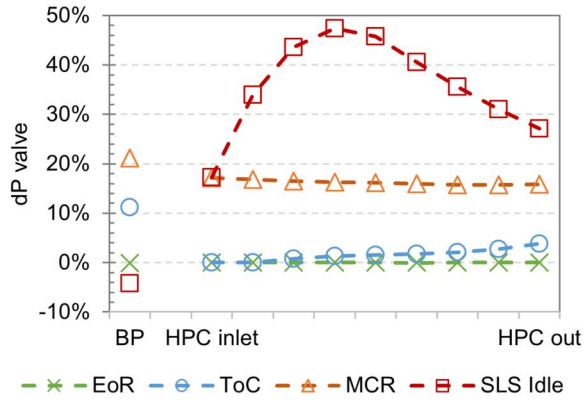

Fig. 12 Pressure control valve losses for various operating conditions against bleed source position

Table 6 Shaft speed change compared to Jet A-1 for the PHC cycle with BP, HPC inlet, and outlet source

Shaft	LP	HP
HP inlet source	+0.4%	+13.3%
HP outlet source	+0.3%	+2.7%
BP source	+0.2%	+0.3%

6 Reconfiguring for Operation Within Jet A-1 Certified Limits

Every NGV comes with its inner-wall and outer-wall platforms. Based on industrial experience, during the manufacturing process, the platform width and available material is such that it allows for a limited NGV rotation around a pivot point typically within a few degrees around its baseline. The margin is built-in to accommodate small changes in the HPT cascade throat area and associated capacity of the order of ±3% during the engine development program, as a means of optimizing development-engine performance prior to certification. In the modeling context, the effect of the turbine NGV is captured by introducing modifications to the Wc scaling factors of the turbine maps (s_{Wc}). The effect of modifying the Wc of the turbine on the efficiency of the component is considered minimal and is not considered.

The core nozzle area can also be realistically modified, via a change in the hot nozzle cone diameter, while maintaining the cone angle within acceptable limits. It features the advantages of being a static metallic component utilizing established manufactured approaches. The change in hot nozzle area affects the LPT expansion ratio and power, hence the residual hot-nozzle PR ratio and the hot-stream jet velocity.

The objective is to find a combination of the two aforementioned factors that either match or even further reduce the shaft rotational speeds to the equivalent Jet A-1 values. As there is a range of solutions that satisfy the above constraints, the final configuration is selected with the view of allowing adequate speed and temperature margins as a means of recognizing the uncertainty of the modeling and the assumptions made. The A_{core} is investigated within the range of 0 to −15% of its baseline value, while the s_{Wc} between ±3%. The change in N_{HP}, N_{LP}, and TET delta at EoR compared to the Jet A-1 performance are presented in Figs. 13–15. Additionally, differences in ESFC compared to the baseline cycle are presented in Fig. 16.

Decreasing the A_{core} restricts the mass flow into the core and enables the LPC to rematch while at almost constant LP speed at a thrust, hence affecting the LPC-HPC PR split. Changing the HPT capacity further affects HPC rematching. A potential HPC working line shift toward the surge line is restricted by a minimum allowable surge margin.

A feasible solution space is determined, where both shaft mechanical speeds are within the limits imposed by the maximum EoR values of the Jet A-1 cycle. The feasible configuration space considers an increase in HPT capacity (s_{Wc}) between 1.2 and 3%

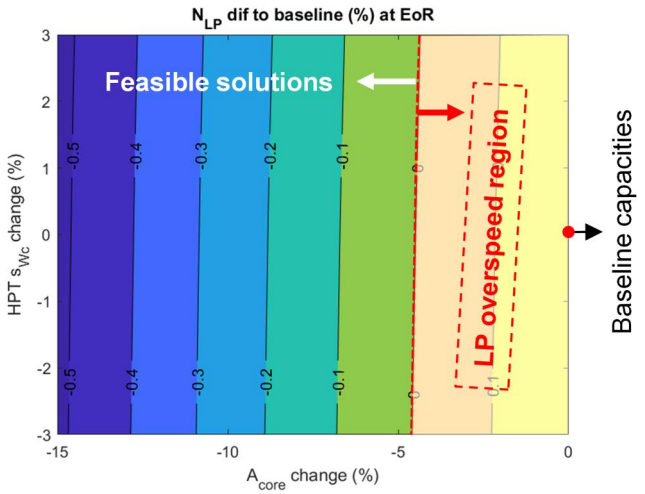

Fig. 14 N_{LP} relative difference between PHC and Jet A-1 at EoR over core parameter reconfiguring

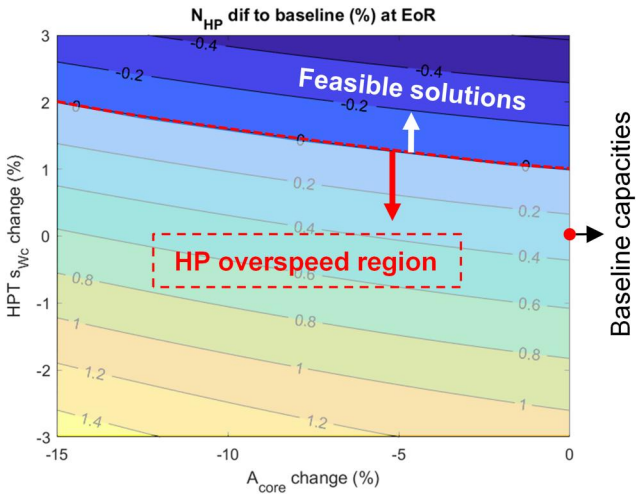

Fig. 13 N_{HP} relative difference between PHC and Jet A-1 at EoR over core parameter reconfiguring

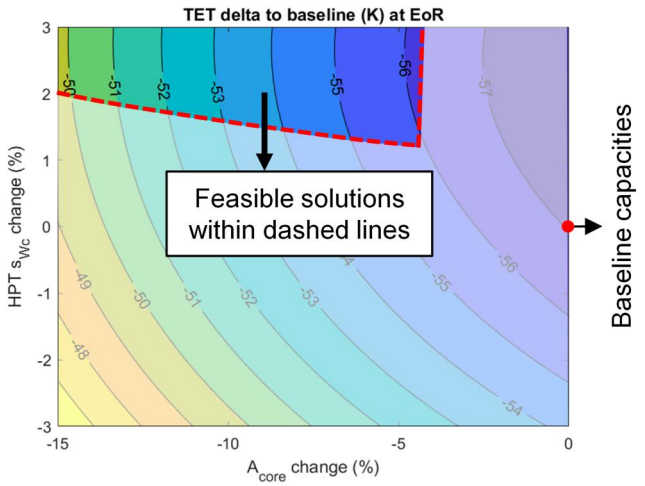

Fig. 15 Turbine entry temperature deltas between PHC and Jet A-1 at EoR over core parameter reconfiguring

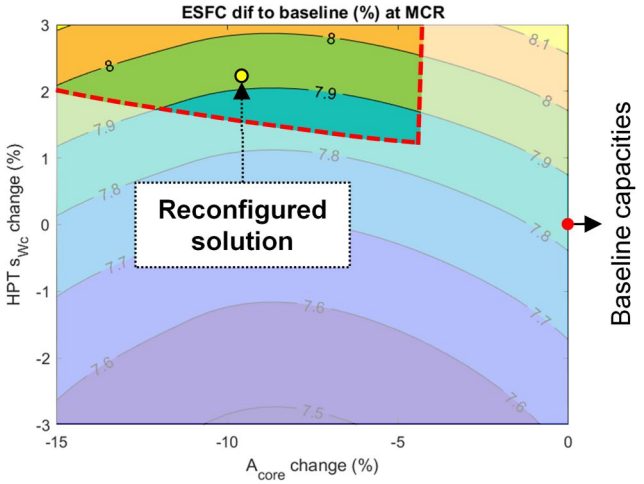

Fig. 16 Energy specific fuel consumption difference to baseline for the PHC at MCR over core parameter reconfiguring

Table 7 Engine core reconfiguring results—differences to Jet A-1 baseline

Parameter	GH_2[a]	PHC BP base	PHC BP reconfigured
A_{core} change	0%	0%	−9.5%
s_{Wc}	0%	0%	+2.2%
TET (K) delta PHC versus Jet A-1 at EoR	−63	−57	−53.5
N_{HP} at EoR	+0.7%	+0.3%	−0.21%
N_{LP} at EoR	+0.1%	+0.2%	−0.24%
ESFC relative PHC versus Jet A-1 at MCR	−1.7%	+7.8%	+7.9%

[a]Performance differences for GH_2 without fuel conditioning.

(see Fig. 13) and a reduction in A_{core} (see Fig. 14) of at least 4.5%. The increase in the HPT capacity favors an HPC working line drop away from the surge line, which counteracts the HPC working line rise that was caused by the change in combustion-product gas-properties, when switching from Jet-A1 to H_2. Decreasing the A_{core} is a way of restricting power to the LP shaft, reducing mechanical LP speed and accommodating the drop in bypass thrust via an increase in core thrust. As demonstrated in Sec. 5.3, the PHC with the BP bleed allows for a significant TET margin at EoR. By reconfiguring the examined parameters, all the feasible solutions are also well below the TET limits, as shown in Fig. 15.

Considering the above a solution is identified that is centered in the feasible reconfiguration space, allowing for adequate margins to the overspeed region of both shafts. Its performance difference to the baseline is presented in Table 7 together with the initial PHC BP cycle before any reconfiguration and the case of the GH_2 cycle without conditioning as discussed in Sec. 4. The ESFC penalty at MCR after the parameter change is only increasing by 0.1%, without any reconfiguration, whereas both shafts reduce their respective speeds at EoR by a little over 0.2%.

Real-life examples may feature different thrust ratings and temperature limits to the ones considered in this study. However, the principle has been demonstrated that the HPT and core nozzle capacities can be modified for constraining HP and LP mechanical speeds within their maximum certified values, while optimizing for MCR fuel burn in a retrofitting scenario.

7 Conclusions

The paper carried out a preliminary exploration of the operational envelope of a kerosene-based civil turbofan engine retrofitted with a LH_2 preheater system, considering various bleed locations for its air supply. The study concludes on the following points:

1. Sourcing PHC air from the core is not recommended. Selecting a core compressor bleed as the PHC source would result in the introduction of additional systems to exploit the high thermodynamic properties of the preheater exhaust gases for generating useful thrust and/or power at preheater exhaust. Otherwise, the high potential thermodynamic properties would be wasted resulting in the demonstrated drop in thermal efficiency. The significant drop in thermal efficiency would most likely have to be compensated via a core size increase for the purposes of generating the same thrust duty within engine mechanical and temperature limits; a core size increase being a design change at engine rather than system level. Cascading consequences emerge regarding weight, design scope and complexity, which lend themselves to a launch of a new engine with consequences on development timescales, costs and risk.
2. Sourcing air from the bypass stream is favorable as it allows the pre-heater to exhaust via existing ventilation nozzles, which would need to be adapted accordingly. Additionally, the interaction of the preheater with the core engine is considerably reduced. A bypass PHC air-source does not severely infringe the validity of assumptions made in Sec. 2, to the extent that the conclusions of this section are invalidated.
3. Combustion products of air with H_2 and their gas properties have been shown to re-match the core engine, in terms of turbine expansion ratios and compressor operating points, with likely cascading effects on turbine and air-system attributes. However, the magnitude of such change may be accommodated by changes within the existing Turbines and secondary air systems, rather than architectural changes. As such, it has been shown that the engine can meet its thrust duty within certified mechanical and temperature limits by realistic changes in the capacities of the HPT and hot nozzle. The HPT capacity change demonstrated is restricted within the traditional ±3% margin accommodated in an engine development program and reflected in the HPT design and manufacturing drawings. It is at the discretion of the engine manufacturer whether the hot section requires three-dimensional airfoil optimization of the stator vanes and/or rotor blades, depending on the efficiency loss associated with a simple geometric re-staggering of the HPT NGVs and the magnitude of turbine operating point rematching. Adjustment of secondary air-system flows for the purposes of turbine cooling, turbine rim sealing and bearing load management will result from adjustment of secondary air-system flow restrictors, seal radii and gaps using the same compressor manifolds.
4. If gaseous hydrogen was readily available to the engine, the engine energy consumption would improve at the same propulsive work by approximately 1.7% relative to Jet-A1. This is attributed to the increased heat capacity and gas constant of the combustion products of air with hydrogen.
5. When the conditioning of liquid hydrogen is carried out by the engine, it fully compensates for the favorable effects of exhaust gas properties. Energy consumption at the same propulsive work deteriorates by approximately 7.9% relative to Jet A-1; that is with the PHC sourcing air from the bypass stream as the least penalizing option. The 7.9% deterioration in energy use for the same thrust duty is a preliminary estimate and does not include any potentially penalizing effect of the assumptions made.
6. While the study is using a geared turbofan architecture as a test-case, the thermodynamic response will be similar for a direct-drive high-bypass-ratio civil turbofan, albeit the exact figures may change, when considering: (a) a bypass air-source for the PHC, (b) the gas properties of exhaust gases of air and H_2, and (c) the proposed capacity changes.

With the bypass stream being recommended as the PHC air-source, the following requirements emerge with recommendations for further work:

- A solution is required to resolve the supply of air to the PHC at SLS idle conditions, whereby the fan pressure rise is inadequate.
- A solution is required for significantly reducing the increased physical size of the preheater.

The recommendations and proposed work aim at an informed concept down-selection for the PHC air-source location, while recognizing that detailed design will have to address the assumptions summarized in Sec. 3 across the engine flight envelope.

Acknowledgment

The authors are grateful to Rolls-Royce plc for its support during the project. The authors confirm that the data supporting the findings of this study are available within the article.

Funding Data

- ATI/iUK (UKRI, PINES project — Reference No. 113263; Funder ID: 10.13039/501100006041).

Data Availability Statement

The datasets generated and supporting the findings of this article are obtainable from the corresponding author upon reasonable request.

Nomenclature

A = area
BPR = by-pass ratio
CC = combustion chamber
CEA = chemical equilibrium compositions and applications
Cp = specific heat capacity
D = diameter
DP = design point
ECS = environmental control system
EoR = end of runway
ER = expansion ratio
ESFC = energy specific fuel consumption
FAR = fuel-to-air ratio
FPR = fan pressure ratio
GH_2 = gaseous hydrogen
h = specific enthalpy
HP = high pressure
HPC = high-pressure compressor
HPT = high-pressure turbine
HTR = hub-to-tip ratio
ISA = international standard atmosphere
LHV = lower heating value
LP = low pressure
LPC = low pressure compressor
LPT = low pressure turbine
MCR = mid-cruise
Mn = Mach number
NASA = National Aeronautics and Space Administration
Nc = corrected rotational speed
NPR = nozzle pressure ratio
OD = off-design
OPR = overall pressure ratio
P = total pressure
PC = primary combustor
PHC = parallel hydrogen combustion
PR = pressure ratio
PW = power
q = heat flow rate
R = gas constant
s = map scaling factor
SC = secondary combustor
SFC = specific fuel consumption
SLS = sea level static
SMR = short-to-medium range
T = total temperature
T3 = HPC exit temperature
TET = turbine entry temperature
ToC = top of climb
V = velocity
VIGV = variable inlet guide vanes
VSV = variable stator vanes
W = mass flow rate
Wc = corrected mass flow rate
WF = fuel flow rate
γ = specific heat ratio

References

[1] Brewer, D., 1990, *Hydrogen Aircraft Technology*, CRC Press, Boca Raton, FL.
[2] Airbus Deutschland GmbH, 2003, *Liquid Hydrogen Fuelled Aircraft – System Analysis*, CRYOPLANE Project, Airbus Deutschland GmbH, Hamburg, Germany, Contract No. G4RD-CT-2000-00192.
[3] Westenberger, A., 2003, "Hydrogen Fueled Aircraft," AIAA Paper No. 2003–2880.
[4] Sethi, V., Sun, X., Nalianda, D., Rolt, A., Holborn, P., Wijesinghe, C., Xisto, C., et al., 2022, "Enabling Cryogenic Hydrogen-Based CO_2-Free Air Transport: Meeting the Demands of Zero Carbon Aviation," IEEE Electrification Mag., **10**(2), pp. 69–81.
[5] Verstraete, D., 2009, "The Potential of Liquid Hydrogen for Long-Range Aircraft Propulsion," Ph.D. dissertation, School of Engineering, Cranfield University, Bedford, UK.
[6] Abedi, H., Xisto, C., Jonsson, I., Grönstedt, T., and Rolt, A., 2022, "Preliminary Analysis of Compression System Integrated Heat Management Concepts Using LH_2-Based Parametric Gas Turbine Model," Aerospace, **9**(4), p. 216.
[7] Huete, J., Nalianda, D., and Pilidis, P., 2021, "Propulsion System Integration for a First-Generation Hydrogen Civil Airliner?," Aeronaut. J., **125**(1291), pp. 1654–1665.
[8] Palmer, C. J., 2024, "Hydrogen Fuel Vaporiser," Patent Application No. 17,487,575.
[9] Tacconi, J., and Grech, N., 2023, "Advanced Hydrogen Cycles to Help Decarbonize the Aviation Industry. Part 1: Development of Simulation & Modeling Toolsets," ASME Paper No. GT2023-103505.
[10] Boehm, R. C., Yang, Z., Bell, D. C., Feldhausen, J., and Heyne, J. S., 2022, "Lower Heating Value of Jet Fuel From Hydrocarbon Class Concentration Data and Thermo-Chemical Reference Data: An Uncertainty Quantification," Fuel, **311**, p. 122542.
[11] Gordon, S., and McBride, B., 1994, "Computer Program for Calculation Complex Chemical Equilibrium Compositions and Applications. Part 1 Analysis,"NASA Lewis Research Center, Cleveland, OH, accessed Dec. 6, 2023, https://ntrs.nasa.gov/citations/19950013764
[12] STO/NATO, 1995, "Recommended Practices for the Assessment of the Effects of Atmospheric Water Ingestion on the Performance and Operability of Gas Turbine Engines," AGARD AR No. 332, accessed Dec. 7, 2023, https://www.sto.nato.int/publications/Pages/default.aspx
[13] Volponi, A. J., 1999, "Gas Turbine Parameter Corrections," ASME J. Eng. Gas Turbines Power, **121**(4), pp. 613–621.
[14] Aretakis, N., Roumeliotis, I., Alexiou, A., Romesis, C., and Mathioudakis, K., 2015, "Turbofan Engine Health Assessment From Flight Data," ASME J. Eng. Gas Turbines Power, **137**(4), p. 041203.
[15] Athanasakos, G., Aretakis, N., Alexiou, A., and Mathioudakis, K., "Turboelectric Distributed Propulsion Modelling Accounting for Fan Boundary Layer Ingestion and Inlet Distortion," ASME Paper No. GT2020-14621.
[16] Alexiou, A., Aretakis, N., Roumeliotis, I., Kolias, I., and Mathioudakis, K., 2017, "Performance Modelling of an Ultra-High Bypass Ratio Geared Turbofan," 27th International Society for Air Breathing Engines, Manchester, UK, Sept. 3–8, Paper No. ISABE-2017-22512.
[17] Bellocq, P., Sethi, V., Cerasi, L., Ahlefelder, S., Singh, R., and Tantot, N., 2010, "Advanced Open Rotor Performance Modelling for Multidisciplinary Optimisation Assessments," ASME Paper No. GT2010-22963.
[18] Mastropierro, F. S., Sebastiampillai, J., Jacob, F., and Rolt, A., 2020, "Modeling Geared Turbofan and Open Rotor Engine Performance for Year-2050 Long-Range and Short-Range Aircraft," ASME J. Eng. Gas Turbines Power, **142**(4), p. 041016.
[19] Alexiou, A., Aretakis, N., Kolias, I., and Mathioudakis, K., 2021, "Novel Aero-Engine Multi-Disciplinary Preliminary Design Optimization Framework Accounting for Dynamic System Operation and Aircraft Mission Performance," Aerospace, **8**(2), p. 49.
[20] Van Heerden, A. S. J., Ippedico, S., Rajendran, D. J., Anselmi-Palma, E., Roumeliotis, I., Pachidis, V., Sharpe, R., et al., 2023, "Performance Analysis of an Engine-Mounted Compression System for Aircraft Environmental Control," ASME Paper No. GT2023-100761.
[21] Walsh, P. P., and Fletcher, P., 2004, *Gas Turbine Performance*, Blackwell Science, Oxford, UK.
[22] NIST, 2020, "Thermophysical Properties of Fluid Systems," National Institute of Standards and Technology, Gaithersburg, MD, accessed Oct. 30, 2020, https://webbook.nist.gov/chemistry/fluid/

https://dspace.org/

Assessment of a liquid hydrogen conditioning system for retrofitting on kerosene designed turbofans

Rompokos, Pavlos; Kyritsis, Vasileios; Mourouzidis, Christos; Roumeliotis, Ioannis

2025-10-01
American Society of Mechanical Engineers (ASME)
https://doi.org/10.1115/1.4067915
Rompokos P, Kyritsis V, Mourouzidis C, Roumeliotis I. (2025) Assessment of a liquid hydrogen conditioning system for retrofitting on kerosene designed turbofans. Journal of Engineering for Gas Turbines and Power, Volume 147, Issue 10, October 2025, Article number 101003, Paper number GTP-24-1679

Downloaded from a DSpace repository. https://dspace.org/